ELSEVIER

Earth and Planetary Science Letters 201 (2002) 431–446

EPSL

www.elsevier.com/locate/epsl

Natural hydraulic cracking: numerical model and sensitivity study

Xiaorong Luo [a], Guy Vasseur [b,*]

[a] *Kay Laboratory of Mineral Resources, Institute of Geology and Geophysics, Chinese Academy of Sciences, Beijing 100029, PR China*
[b] *SISYPHE, UM7619, Boîte 123, Université Paris 6, 75252 Paris Cedex 05, France*

Received 13 December 2001; received in revised form 23 April 2002; accepted 2 May 2002

Abstract

Natural hydrofracturing caused by overpressure plays an important role in geopressure evolution and hydrocarbon migration in petroliferous basins. Its mechanism is quite well understood in the case of artificial hydraulic fracturing triggered by high-pressure fluid injection in a well. This is not so for natural hydraulic fracturing which is assumed to initiate as micro-cracks with large influence on the permeability of the medium. The mechanism of natural hydraulic cracking, triggered by increasing pore pressure during geological periods, is studied using a fracturing model coupled to the physical processes occurring during basin evolution. In this model, the hydraulic cracking threshold is assumed to lie between the classical failure limit and the beginning of dilatancy. Fluid pressure evolution is calculated iteratively in order to allow dynamic adjustment of permeability so that the fracturing limit is always preserved. The increase of permeability is interpreted on the basis of equivalent fractures. It is found that fracturing is very efficient to keep a stress level at the rock's hydraulic cracking limit: a fracture permeability one order of magnitude larger than the intrinsic permeability of the rock would be enough. Observations reported from actual basins and model results strongly suggest that natural hydraulic cracking occurs continuously to keep the pressure at the fracturing limit under relaxed stress conditions.

Keywords: basins; overpressure; hydrodynamics; fractures permeability; numerical models

1. Introduction

The pore pressure within sedimentary basins may become very large, even close to, but rarely above the vertical lithostatic stress [1–4]. Before pore pressures reach lithostatic stress, fractures appear and release some pore fluid. This phenomenon, called 'natural hydraulic fracturing' (NHF) [1,5] to distinguish it from the hydraulic fracturing resulting from the injection of pressured fluids into the borehole [6–8], therefore provides a limitation on the pore pressure within sedimentary basins.

Most of our knowledge about hydrofracturing comes from oil well hydraulic fracturing where the concept of effective stresses is successfully applied [9–12]. Hubbert and Willis [9] first synthesized the mechanics of hydraulic fracturing. They

* Corresponding author.
E-mail addresses: xrxuluo@public.bta.net.cn (X. Luo), vasseur@biogeodis.jussieu.fr (G. Vasseur).

0012-821X/02/$ – see front matter
PII: S0012-821X(02)00711-2

discussed the effect of increasing pore pressure on underground stress state and analyzed the stress field around a borehore when high-pressure fluid is injected into one permeable formation. They observed that fractures occur along planes normal to the least principal stress when the pressure of the injected fluid reaches the least principal stress. The concept of hydraulic fracturing was then applied to field data to explain the natural formation and propagation of joints [5,13].

Engelder and Lacazette [5] noted two important differences between NHF and oil well hydraulic fracturing (OWHF). Firstly, in OWHF the fluid pressure in the borehole is different from the pore pressure behind the borehole wall (to make sure the pressure in the borehole actually reaches the fracturing threshold, the pumped pressure is usually higher than the surrounding value). Secondly, the crack driving stress for OWHF does not drop once the fractures appear in the well since the borehole is continually being charged.

Numerical basin models that integrate such natural hydrofracturing have been developed [14–16]. They usually consider a threshold on pore pressure magnitude, typically of the order of least principal stress [9], above which a fracture or a network of fractures that cut through the whole sealing layer is assumed to open at once with a given aperture or permeability [2,4,17,18]. As a consequence, the pore pressure decays rapidly below the threshold and the fracture is assumed to close. If the source of overpressure is maintained, the process is repeated episodically [2,17].

Following our previous modeling works as well as others [2], we observe that in some peculiar conditions the modeled pore pressures may be locally very high, as illustrated in Fig. 1. Therefore, we conjecture that a connected array of micro-cracks is generated at, and only at, the locations where some threshold is reached (Fig. 1). These micro-cracks would originate at existing flaws and tend to generate locally a hydraulic connection: this connection does not require fully developed macroscopic hydrofractures and does

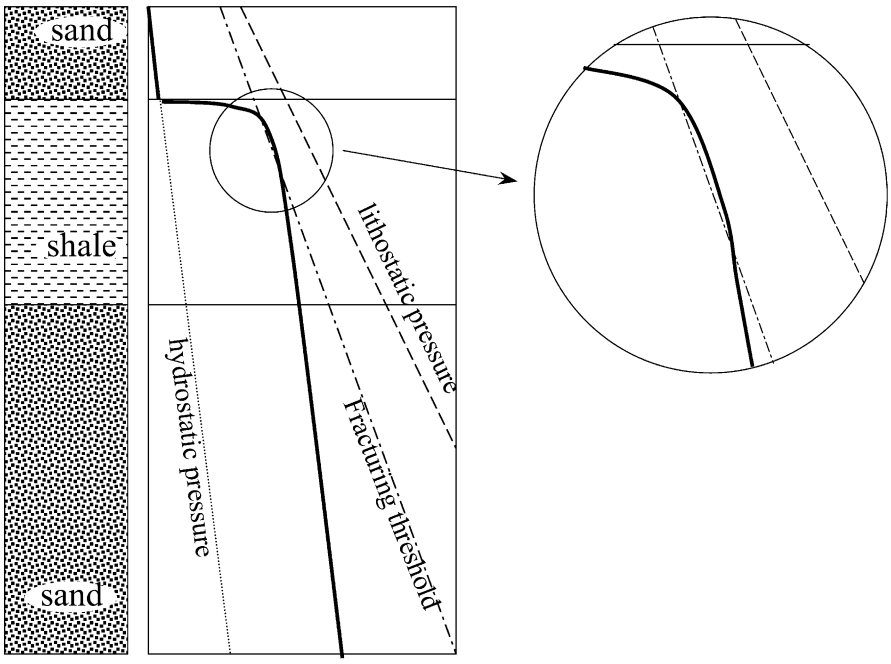

Fig. 1. Modeled pore pressure distribution in a 1D profile in which one low permeable shale is sandwiched between two sand beds. The compaction in both the shale and the sand formation beneath may generate important pore pressure. The pressure may slightly exceed the fracturing threshold at the upper part of the shale because no correction for fracturing was introduced in the calculation.

not necessarily cut through whole layers at once, as suggested by Nunn [19]. As a consequence, rapid pressure readjusting occurs only within this fractured part and coupled with the fracturing process.

We assume that this hydromechanical process does occur in shale formations. This assumption seems sound because shales are major sources of overpressures [1,21,22], and often behave as sealing formations [1,2,17]. Also, in shales, the distribution of the overpressures in a shale is usually not homogeneous [1,20], (Fig. 1) which favors the fracturing process. In order to distinguish this concept from OWHF [9] and from NHF, the phenomenon generating such micro-cracks will be referred to as natural hydraulic cracking (NHC) throughout this paper.

Besides the two differences emphasized by Engelder and Lacazette [5] between OWNF and NHF, some other differences between NHC and OWHF and/or NHF should be taken into account. For example, NHC occurs in shale formations where the permeability is very small, whereas OWHF is generally performed in more permeable beds and NHF may propagate through both beds. We assume that the pressure increase generating NHC is a slow process occurring at geological time scale whereas the pressure variations are very fast in OWHF (humans are generally impatient); for NHF, the tectonic stress is usually the trigger whereas overpressures in pores decrease only the strength of rocks. Lastly, as a result of the above differences, the fracture size of NHC is likely much smaller than that caused by OWHF and NHF. These property differences from OWHF and NHF seem to favor the idea that the NHC is some kind of subcritical process [24] occurring quasi-continuously near equilibrium [25].

This paper uses a one-dimensional numerical model to analyze these effects by introducing an iterative method to follow the coupling between pressure readjustment, compaction and fracturing. When the fracturing pressure threshold is reached, the permeability created by these new micro-fractures is iteratively computed so as to keep the pressure at the threshold. We show that under these conditions a continuous release of pore pressure is possible and we analyze the sensitivity of these results to varying states of stress, tensile strength and sources of overpressures.

2. Natural hydraulic cracking modeling

Our model is based on the recognition that the micro-cracks appear for stress and pressure states close to some kind of equilibrium state and that the permeability associated with these micro-cracks maintains the pore pressure close to the fracturing threshold. An iterative method is therefore developed to compute this fracture permeability.

2.1. Cracking criterion

Mechanically, when the effective stresses decrease as a result of abnormal fluid pressure, more and more micro-cracks may appear in the sediments (tensile or shear). This process corresponds to the dilatant stage of the rock deformation laboratory tests [26,27]. With the increase of micro-crack density, more and more micro-cracks connect one to another. In the three-dimension space, when a sufficient number of micro-cracks become connected in a given unit of rock, they form a cluster allowing the fluid to flow through the unit whereas the rock does not fail (Fig. 2). This is one kind of percolation process that has been discussed by Gueguen and his co-workers [28,29]. A recent paper [29] provides a quantitative approach of permeability enhancement associated with micro-crack occurrence related to dilatancy.

Failure is preceded by dilatancy. Within the dilatant stage, micro-cracks appear dominantly at positions where flaws exist. At the micro-scale, the existence of these cracks makes sediments heterogeneous, whereas at a larger scale, the distribution of the cracks may be regarded as homogeneous. Brace et al. [26] showed that the differential stress value at the beginning of the dilatancy is proportional to that at failure threshold. The envelope for natural hydraulic cracking is thus taken as a belt parallel to the failure enve-

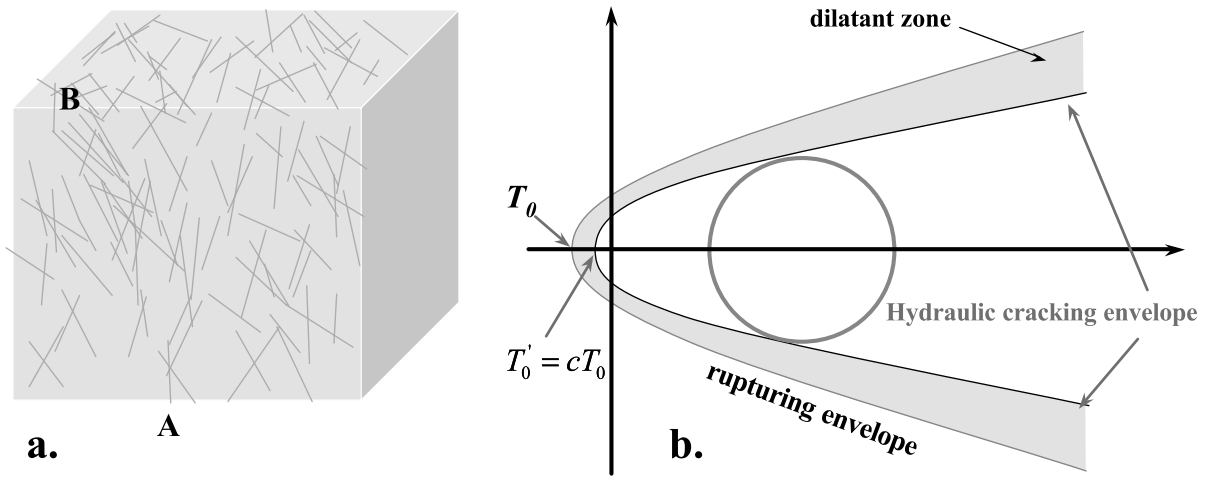

Fig. 2. The concepts of hydraulic cracking (a) and corresponding criterion (b). Note in diagram b, the hydraulic cracking criterion is similar in shape to the modified Griffith failure criterion [30], falling in the dilatant zone defined by [27].

lope corresponding to the dilatant zone in Mohr's representation (Fig. 2, after [27,30]).

Many experiments have shown that the failure criterion of muddy rocks under confining stress conditions may be described by the modified Griffith criterion [12,31,32]. Handin et al. [31] tried to do similar failure experiments by increasing pore pressure in muddy rocks. They failed because the permeability of the muddy samples is too low to allow pore pressure re-equilibration during a short experiment period.

Here we are concerned with a stress regime where overpressured shale has been consolidated and even overconsolidated (it was subjected to a maximum effective stress larger than the present one). Under these conditions, it should be suitable to apply these experimental results to our simulation work. The criterion for micro-fracturing is thus defined as a modified Griffith criterion [26,12,30,31,33].

$$\begin{aligned} \tau^2 &= 4T'_0\sigma' + 4T'^2_0 \quad \text{when} \quad \sigma' < \frac{1-\mu^2}{\mu}T'_0 \\ \tau &= \frac{1-\mu^2}{\mu}T'_0 + \mu\sigma' \quad \text{when} \quad \sigma' > \frac{1-\mu^2}{\mu}T'_0 \end{aligned} \tag{1}$$

where σ' and τ are respectively the normal effective stress and the shear stress acting on an arbitrary plane in the rock, $\mu = tg\theta$ the friction coefficient, in which θ is the internal friction angle, $T'_0 = aT_0$ is the tensile strength of the rock corresponding to cracking, and T_0 the tensile strength of the rock, a a constant smaller than 1.0, depending on the sample material as well as the ambient conditions [26]. Depending on where the Mohr circle touches the micro-cracking envelope, tensile cracks or shear cracks would occur.

2.2. Fracture porosity and permeability

In order to be able to calculate the value of the fracture porosity, we assume that the fracture porosity is only associated with the micro-cracks that constitute the percolation cluster. Isolated micro-cracks that do not drain fluid will be assumed to be closed ones. This fracture concept is illustrated in Fig. 3. For a sediment layer, we assume that micro-cracks are parallel planes crossing the layer with the same aperture b. For a cubic elementary volume with size w, volume $V = w^3$ and face area $A = w^2$, we call L the equivalent horizontal fracture length.

Based on the work of Snow [34], Sagar and Runchal [35] among others, the permeability of a parallel plate fracture is calculated as:

$$k_f = \frac{b^3}{12}\frac{L}{A} \tag{2}$$

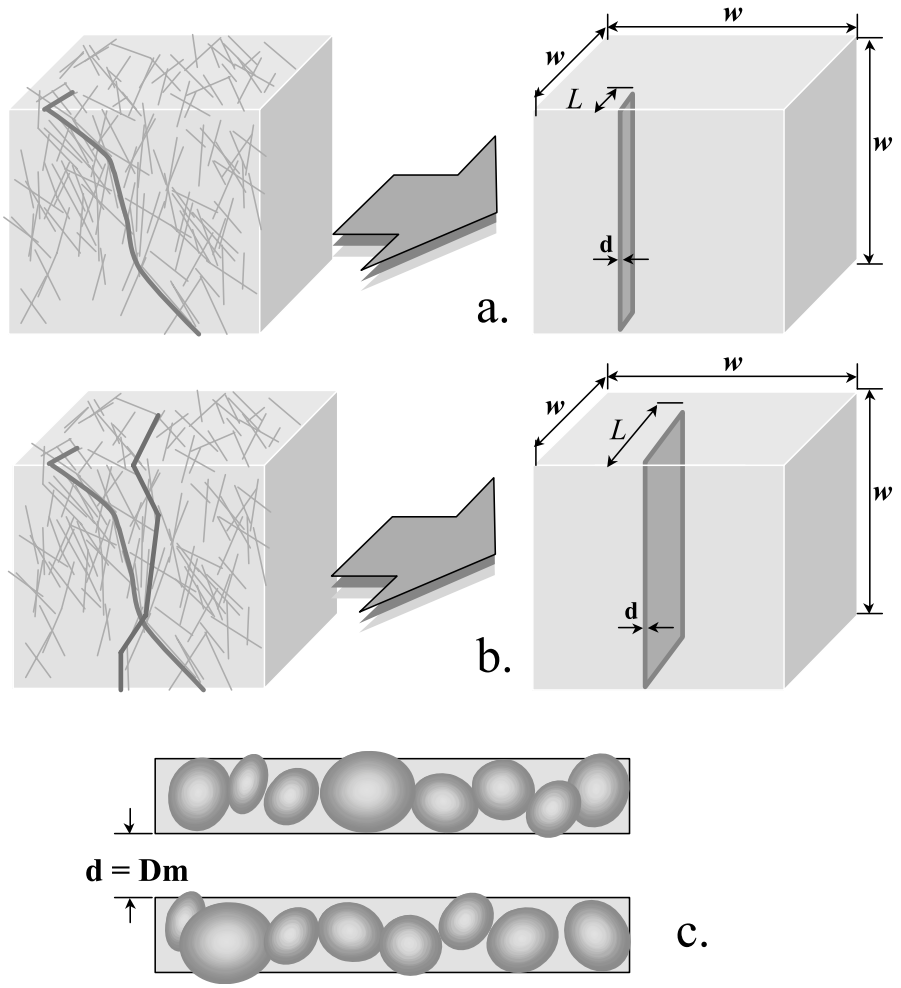

Fig. 3. The porosity related to micro-cracks can be calculated by assuming a plane fracture of length L. (a) At the fracturing threshold. (b) During the fracturing process. (c) Micro-crack aperture may be assumed as the average diameter of the grains (Dm).

where A is the surface of the section of observing element, L the length of the fracture and b the aperture of the fracture. The equivalent fracture aperture is assumed to be equal to the average diameter of the grains (Dm). With this assumption, the porosity of the fracture can be calculated:

$$\phi_f = \frac{12}{b^2} k_f \tag{3}$$

2.3. Principal stress

The maximum principal stress is assumed to be vertical and equal to the overburden weight. The horizontal principal stress corresponds to the minimum principal stress and is simply taken as a proportion of overburden stress:

$$\sigma_3 = c\sigma_1 \tag{4}$$

where c is a constant usually taken as 0.7–1.0. Engelder and Lacazette [5] argued that it depends

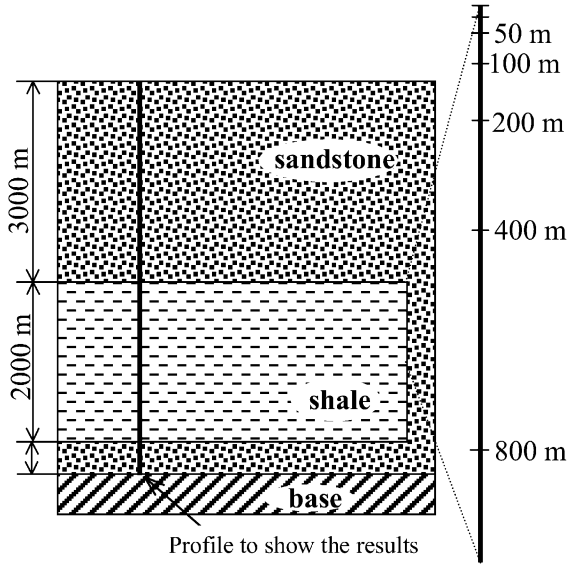

Fig. 4. The profile model. To observe the distribution of pore pressure and to check fracturing at various parts of the shale, the shale is divided vertically into 14 layers with different thickness.

on the Poisson ratio of the sediments, and may reach 0.5 in extreme conditions.

2.4. Lithologies

A simple sediment section is assumed as illustrated in Fig. 4: a shaly formation of 2000 m in thickness is sandwiched between two sandy formations connected by a permeable path at the right of the section that permits the sand beneath the shale to keep at hydrostatic pressure at all times.

Table 1
Parameters used in the fracturing modeling

Symbol	Parameter	Value	Unit
V_0	Sedimentation velocity	350	m Ma^{-1}
f_0	Shale initial porosity	0.65	–
c	Shale compaction coefficient	0.60	km^{-1}
T_f	Surface temperature	15	°C
G_T	Temperature gradient	30	°C km^{-1}
l	Permeability coefficient	2.0×10^{-5}	Darcy
n	Permeability index	5.0	–
E	Activation energy	20.0	kcal mol^{-1}
A	Pre-exponential factor	$4.0\times10^{+10}$	Ma^{-1}

2.5. Source of overpressure

Overpressure is mainly caused by disequilibrium compaction of shaly rocks. However, another important pore fluid source increase stems from organic matter cracking [23] and/or from some other additional sources [36]. To account for these sources, a kinetic process following the Arrhenius formula is introduced in the shale during its burial from 2000 m to 4700 m. Such a kinetic process will generate a fluid source into the shale with a peak value at 3700 m (Fig. 5). The values of the parameters used are listed in the Table 1.

2.6. Numerical approach

To observe the distribution of pore pressure and corresponding fracturing, the shale is divided vertically into 15 layers with different thicknesses (Fig. 4). The thickness of the sand sediments above the shale is 3000 m.

In order to make sure that the fracturing will occur and to control the fracturing process, the hydraulic conditions are carefully designed in the following case studies. The hydraulic conductivity of the shale is determined by choosing the permeability coefficient [22] that would, in the case without fracturing, keep the pore pressure at a value slightly smaller than the fracturing threshold. The additional source of fluid can then generate further overpressure and result in fracturing.

A numerical model developed based on a La-

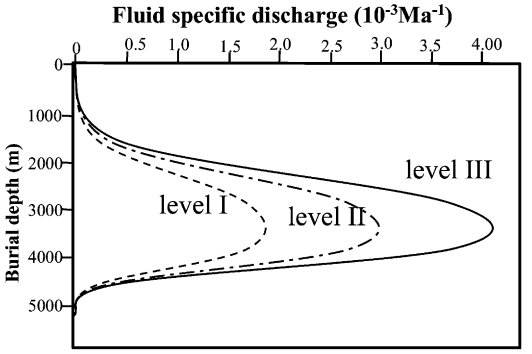

Fig. 5. The fluid specific discharge generated by a kinetic process during the burial history.

grangian finite element approach is used to model the hydraulic cracking process. This model permits us to couple the pressure evolution to the temperature and the compaction of the sediments during the sedimentation [22,23]. Various pressuring mechanisms may be considered in the pressure evolution modeling, such as organic matter cracking, tectonic stressing, as well as clay mineral transformation [20,22,23]. The details about the formula, the algorithm, checking, boundary conditions and parameters can be found in previous work [20,22,23,37].

In our pressuring model, for each calculating step from t_{i-1} to t_i, we first calculate the pressure at the end of the step (t_i); the results are then compared to the fracturing threshold. The excess of pressure with respect to fracturing pressure is obtained: $\Delta P = P - P_f$, where P_f is the fracturing pressure. Fracturing occurs when this pressure excess becomes positive and this results in a fracture

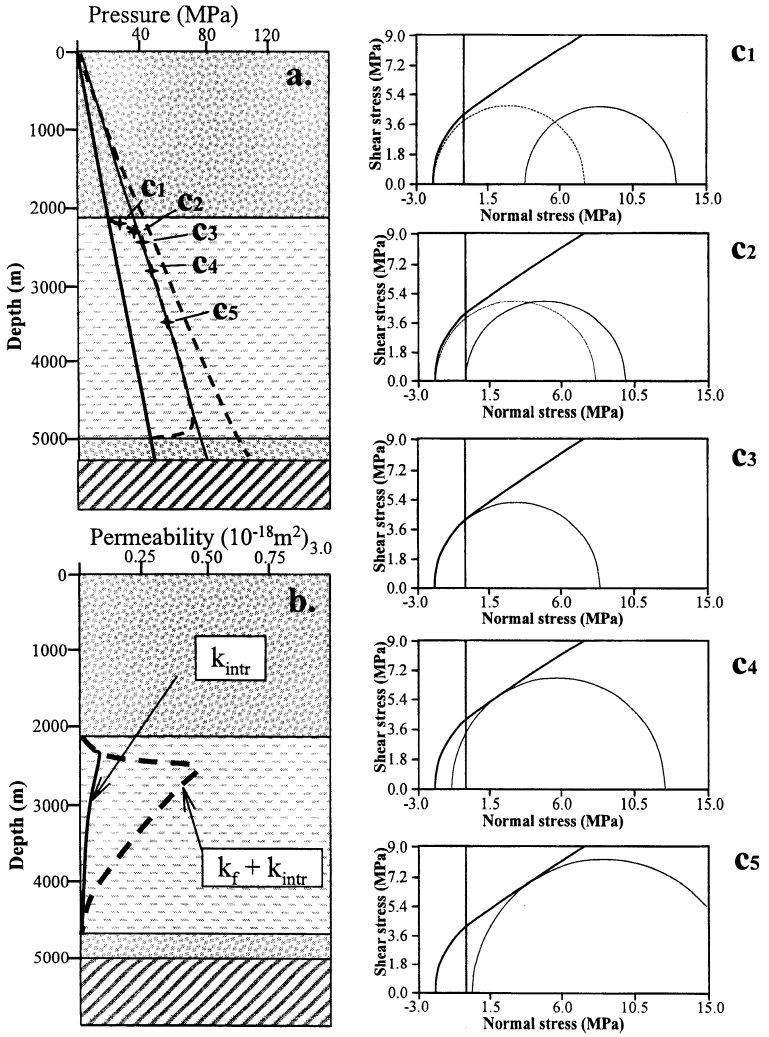

Fig. 6. Modeled results of fracturing happening in the shale. Left: the profiles of the pore pressure (upper) and the permeability in the shale at a specific time (lower, where k_{intr} is the intrinsic permeability and k_f the fracture permeability). Right: the effective stress states at different points marked in the upper left scheme. In diagrams c1 and c2, the dashed circle represents the state where the fracturing happens.

porosity and permeability increase. The porosity created by the fracturing is noted as ϕ_f and the permeability as k_f. During the step, while the fluid corresponding to the pressure increment travels through the fracture, the pore pressure value will stay at the fracturing threshold value.

Numerically these processes are treated iteratively. At the beginning of each step, k_f is given an arbitrary value, slightly larger than that at the last step. The value of ϕ_f is also calculated as explained. Then, a new field of pressure is calculated with these values of k_f and ϕ_f. If the new pressure excess is still positive, then the values of k_f and ϕ_f are increased, and vice versa. The above calculation–comparison process is repeated until the pressure increment obtained from one iteration to the other is smaller than a given slight value, ε.

If at one step, the pressure calculated is smaller than the fracturing threshold, then the opened fractures are assumed to close. To ease the calculation, we assume that the fracture permeability and the corresponding porosity become zero when the fracture is closed [28].

2.7. Results

Fig. 6 illustrates the modeled results on a vertical profile that is situated in the two-dimensional section illustrated in Fig. 4. In Fig. 6, diagram a presents the pressure distribution at a given time, where four pressure curves are included: lithostatic, hydrostatic, fracturing threshold as well as pore pressure. Diagram b illustrates the distribution of permeability corresponding to the pressures in diagram a. In this diagram, the intrinsic permeability and the fracture permeability are presented. Diagram c shows the effective stresses

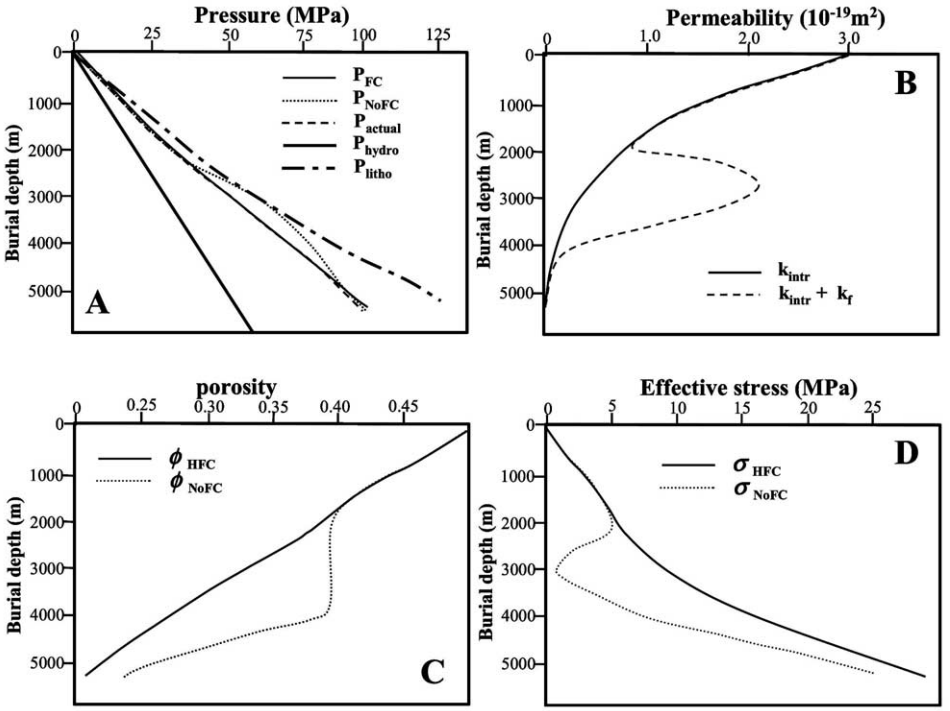

Fig. 7. The trajectories of different parameters at the center of the shale. (A) Pressure evolution, the solid curve presents the fracturing threshold, the fine dotted line the pressure without fracturing correction, and the dashed line the pressure after fracturing correction. (B) The intrinsic permeability (k_{intr}, solid curve) and the total (fracture+intrinsic) permeability ($k_{intr}+k_f$, dashed curve). (C) The porosity with (solid curve) or without (dashed curve) fracturing. (D) The effective stress with (solid curve) or without (dashed curve) fracturing.

state at five points vertically distributed in the shale. Their positions are marked in diagram a. In each scheme, the fracturing envelope and the Mohr circles are illustrated. The solid circle represents the actual stress state and the dotted one the stress state when fracturing would take place.

We note in this figure that when the fracturing occurs in the shale, not the whole shale is fractured. This is because the effective stress states are different at each observing point. At point 1, fracturing does not occur and the Mohr circle is far from the fracturing envelope (c1). At point 2, the stress state stays just below the fracturing as emphasized by the position of the Mohr circle just below the fracturing envelope (c2). Points 3, 4 and 5 are located within the fracturing part, but their stress states are different from each other (c3, c4 and c5). In diagram a, the pressures in the fractured part remain at the fracturing threshold and the corresponding permeability values are larger than the intrinsic one (diagram b), with the largest value at the upper part of the fracturing range.

Fig. 7 shows the trajectories of different parameters at one point located at the center of the shale layer during the burial process. Diagram a shows the evolution of pressures: hydrostatic and lithostatic pressures are respectively presented by solid and dashed curves, the fracturing threshold (P_{FC}) is the fine dashed curve and the pore pressure the fine solid curve. The fracturing potential pressure (the pressure that would occur without accounting for fracturing) is the fine dotted curve. Diagram b presents the permeability: with (dash) or without (dot) fracturing. Diagram c displays the porosity: with (dash) or without (dot) fracturing. Diagram d illustrates the effective stress: with (dash) or without (dot) fracturing.

Comparing the porosity evolution curves in diagram c to the effective stress curves in diagram d, for the case where the fracturing occurs within the 2000–4000 m burial depth interval, the effective stress increases continuously, and then the porosity decreases monotonously as a result of increasing compaction. If the fracturing is not taken into account, the effective stress would tend to decrease with burial depth so that the porosity remains almost constant.

3. Sensitivity study

Within the burial interval from about 2000 m to about 4500 m, the increase of permeability due to fracturing is larger than the intrinsic permeability by no more than one order of magnitude. However, hydraulic cracking is a complex process influenced by many parameters [5]. Sensitivity studies seem to be the best way to analyze the influences of various parameters to the hydraulic cracking process.

Three parameters directly associated with the hydraulic cracking are taken into account. They are respectively: (1) the stress state which is characterized by the ratio of maximum to minimum principal absolute stresses; (2) the tensile strength of rock which gives the possibility of resistance to fracturing; and (3) the pore pressure 'potential' which defines the ability to exceed the fracturing threshold. For each case, only one parameter value is changed. The values of the parameters used in various sensitivity studies are shown in Table 2.

3.1. Source of overpressure

In our models, the generation of high overpressures by a source of fluid injection is a necessary condition for the occurrence of hydrofracturing. This fluid injection is introduced into the shale through a fluid volume increase due to the evolution of organic matter. This is assumed to follow a kinetic process and the parameters used in this kinetic process are listed in Table 1 and the sources introduced for three cases are shown in Fig. 5.

Table 2
The choice of parameters in various cases

Parameter	Case	Fluid source	T_0 (bar)	σ_3/σ_1
Pressure potential	1	**Level I**	15	0.8
	2	**Level II**	15	0.8
	3	**Level III**	15	0.8
Tensile strength	1	Level II	**24**	0.8
	2	Level II	**15**	0.8
	3	Level II	**6**	0.8
Stress state	1	Level II	15	**0.9**
	2	Level II	15	**0.8**
	3	Level II	15	**0.7**

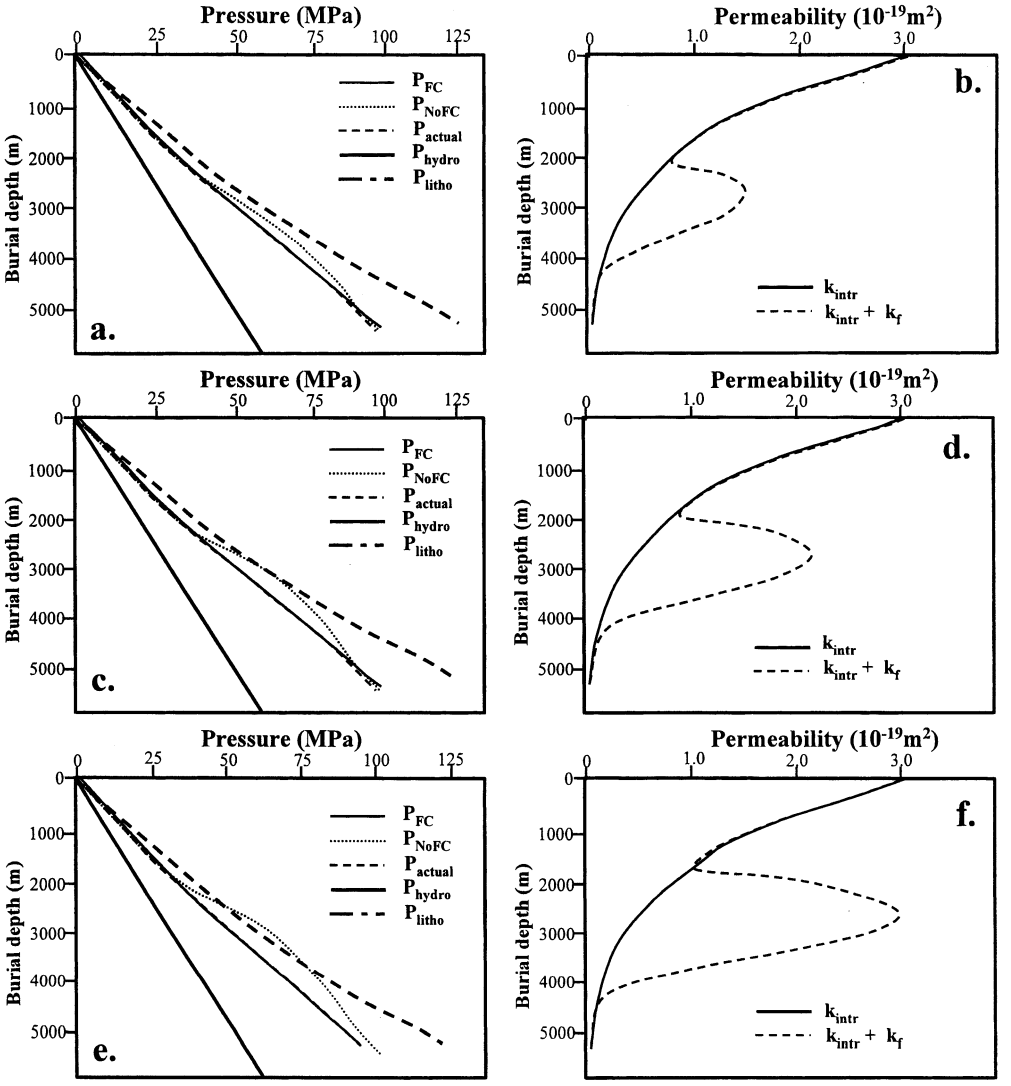

Fig. 8. Effect of hydraulic cracking on pore pressure evolution: the role of fracturing potential. Diagrams a, c and e show pressure evolution at the center of shale by using levels of fluid source augmentation I, II and III, respectively. Diagrams b, d, and f show the intrinsic permeability (k_{intr}) and the total permeability ($k_{intr}+k_f$).

Three levels of fluid injection labelled I, II and III are assumed corresponding to increasing fluid injections.

The influence of the pressuring potential upon the hydraulic cracking is illustrated in Fig. 8. The diagrams a, c and e present the evolution of pressures at the center of the shale by using levels I, II and III of fracturing potential respectively; and diagrams b, d and f present the corresponding permeabilities, taking into account or not fracturing effects.

3.2. The tensile strength

In our model, the resistance of rock to fracture is characterized by the parameter T'_0. In

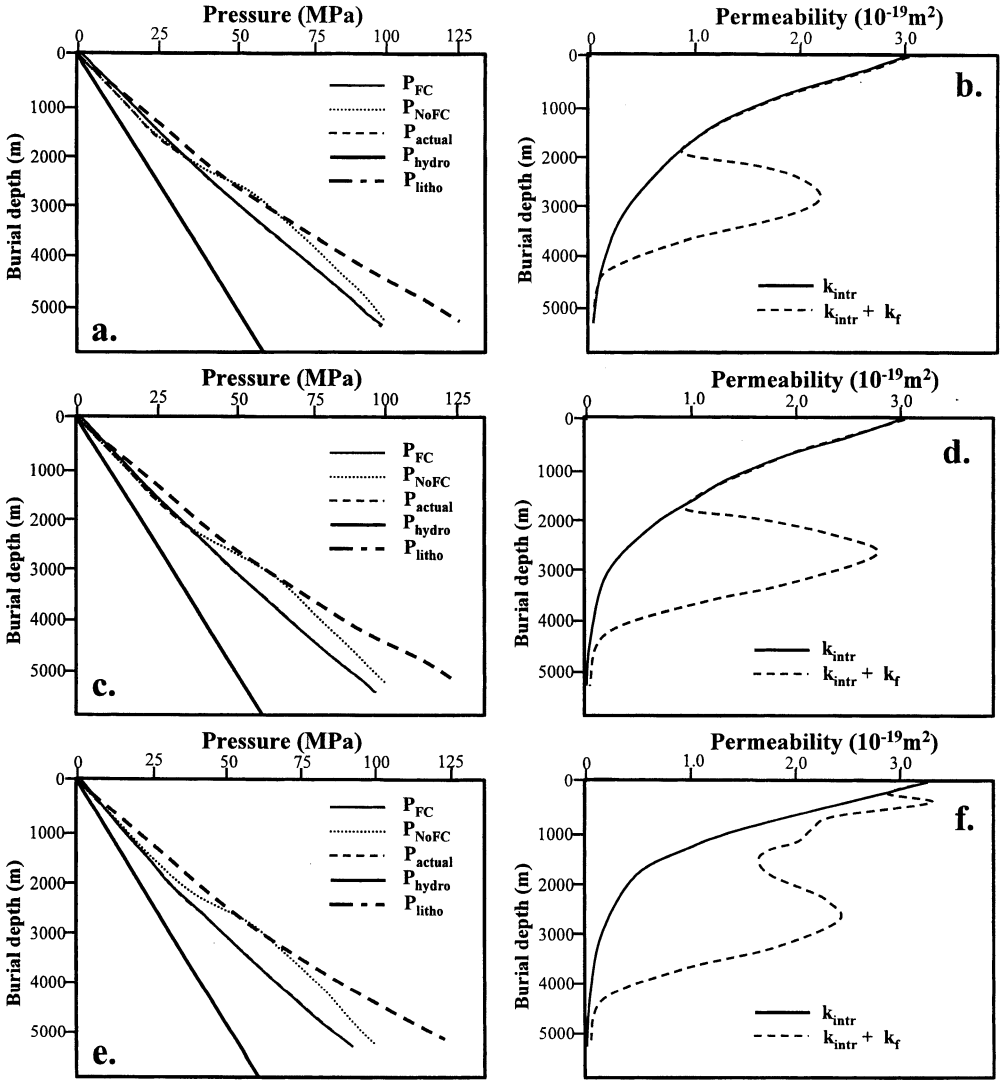

Fig. 9. Effect of hydraulic cracking on pore pressure evolution: the role of T'_0/T_0. Diagrams a, c and e show pressure evolution at the center of shale by using ratios of T'_0/T_0 of 0.7, 0.8 and 0.9, respectively. Diagrams b, d and f show the intrinsic permeability (k_{intr}) and the total permeability ($k_{intr}+k_f$).

Fig. 9, the role of T'_0 on the effect of hydraulic cracking is presented. Diagrams a, c and e present the evolution of pressures at the observing point in the shale by using values of T'_0 of 6, 15 and 24 bars respectively, and diagrams b, d and f present the corresponding values of permeability accounting or not for fracturing.

3.3. State of stress

The stress state varies from area to area. For a tectonically relaxed basin, the horizontal stresses depend on the vertical overburden stress and the rock properties, and the stress rate σ_3/σ_1 is in the range 0.5–1.0 [5,38]. The fracturing threshold is a function of σ_3, σ_1 and pore pressure P (Eq. 2),

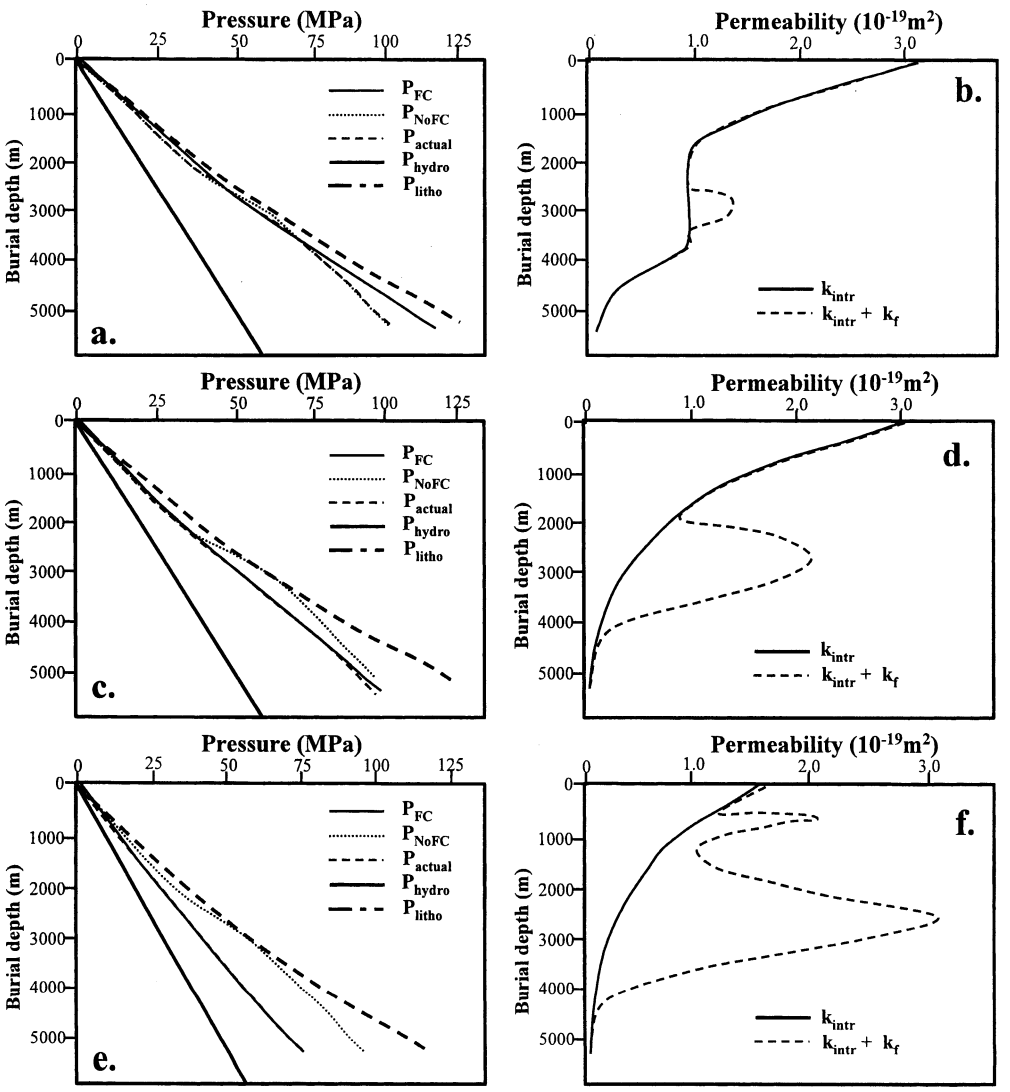

Fig. 10. Effect of hydraulic cracking on pore pressure evolution: the role of σ_3/σ_1. Diagrams a, c and e show pressure evolution at the center of shale by using ratios of σ_3/σ_1 of 0.7, 0.8 and 0.9, respectively. Diagrams b, d and f show the intrinsic permeability (k_{intr}) and the total permeability ($k_{intr}+k_f$).

then the variation of this rate would be important for the hydraulic cracking process.

Similarly Fig. 10 illustrates the role of the σ_3/σ_1 effect of hydraulic cracking on pore pressure evolution. Diagrams a, c and e present the evolution of pressures at the center of the shale when using ratios of σ_3/σ_1 of 0.7, 0.8 and 0.9 respectively; diagrams b, d and f present the values of corresponding permeability when accounting or not for fracturing.

4. Discussion

As a consequence of our assumptions and as illustrated in Figs. 6–10, when fracturing occurs

during the evolution of pore pressure, at some burial interval the pressure remains exactly at the fracturing threshold. Depending on the values of parameters, the burial interval corresponding to fracturing varies from less than 1000 m to more than 4000 m (Fig. 9f). However, in any case, the fracture permeability does not change so much: the increase of permeability is usually limited to one order of magnitude that of the intrinsic one.

In our model, the fracturing is a result of the connection of micro-cracks and the increase of permeability reflects in fact the increasing number of connected micro-cracks. This implies that the opening and the closure of each micro-crack are occurring independently. At micro-scale, the opening of each micro-crack is performed independently. At micro-scale, the opening of each micro-crack is the result of the deformation of the rock under the action of the stress. When effective stress continues to decrease (for example due to increasing fluid pressure or increasing deviatoric stress) then deformation (opening of micro-cracks) occurs that increases micro-crack density and enhances the propagation of the fractures [28]. Reciprocally, it is assumed that open micro-cracks may close completely one by one when stress conditions become different.

For a thick shale layer, the fracturing is not the propagation of open fractures through the shale, but instead, their propagation is limited to a single element layer. Once fracturing occurs in a layer, the pore pressure within the fractured interval is readjusted, which makes the pressure drop at one tip and increase at the other tip. Because the micro-crack density and size involved in the fracturing are very small and therefore very sensitive to pressure variation, such a pressure readjustment may result in the closing of the fracture at the former tip and propagation at another tip. The development of existing fractures depends on the overpressuring potential. If, after pressure readjustment, the pressure tends to increase, then the fracture permeability increases as a result of either an increase in the width of micro-cracks or, more likely, an increase in the density of micro-cracks. The latter possibility (increase of micro-crack density) seems the most likely. When overpressure decreases in a given element, fractures are then allowed to be closed.

4.1. Generation of high overpressures

How may high overpressures be generated in the shales? One extreme possibility is the case of rapid sedimentation rate with a very low permeability in shale [39]. However, such a condition is rarely met in actual basins [3,40]. Recent quantitative studies on overpressuring in shale strongly suggest that high overpressures could be generated by the cumulative effect of compaction plus some other mechanisms [3,23]. The overpressuring mechanisms which are quantitatively proved to be efficient include the cracking of organic matter [23], the external fluid source offered by compacting of thick permeable sediments beneath the observed shale [37] (and as illustrated in Fig. 1) as well as external fluid sources offered by hydraulic connection through open faults [37,41], etc.

4.2. The significance of the dilatant zone

It is well known that in the course of rock rupture laboratory experiments, several stages may be identified under both uniaxial and triaxial conditions [26,27]. After a linear phase where strain is proportional to differential stress, the deformation enters a phase where the volume of the rock tends to increase due to the occurrence of micro-cracks in the rock [12,26,33]. This dilatant phase precedes the final rock failure.

Gueguen and Palciauskas [28] proposed that, during dilatancy, small micro-cracks appear in the rock with increasing differential stress. These micro-cracks are so small that they can close completely if the stress decreases again. When monotonous increase of the stress is imposed, more and more new micro-cracks appear, i.e. their density increases. With increasing micro-crack density, some originally isolated micro-cracks connect one to another. Eventually the micro-crack density become so large that some connected micro-crack clusters appear that allow fracture fluid flow in rock [28].

Experiments associating mechanical deformation and permeability measurements support this

scheme. Zoback and Byerlee [42] measured the relationship between the effective stress and the permeability of the Westerly granite by increasing the effective stress until the dilatancy of the sample occurs. They found that the permeability begins to increase when the dilatancy occurs. During the unloading stage after this, the permeability does not return to its original value, implying that some fractures did not completely close after the stress decrease. However, their further experiments [43] showed that the maintenance of the fracture opening can only be met during the first loading–unloading cycle, if this process is repeated, the newly generated fractures seem to close completely.

4.3. Fracture porosity

The results obtained with the above modeling using Eq. 4 show that the fracturing porosity is very small, varying from 10^{-5} to 10^{-6}. Such a value implies a negligible increase of porosity.

5. Conclusions

The natural hydraulic cracking occurring under tectonically non-active zones is likely to be a near equilibrium continuous process that requires the pore pressure to stay at the fracturing threshold. Based on this idea and using concepts of rock mechanics, the hydraulic consequences of this fracturing process are taken into account by an increase of permeability allowing fluid drainage.

In the investigated case studies we have dealt with, values of fracture permeability do not exceed that of the intrinsic permeability of sediments by more than one order of magnitude. Therefore the increase of permeability by fracturing remains relatively small. But it does efficiently diminish the potential high pressure and keep the pressure at the fracturing threshold. The porosity increase associated with micro-cracking seems to be negligible.

The hydraulic cracking resistance (equivalent to tensile strength for rock failure) is a very important parameter used in the model. It was imposed at a value smaller than the tensile strength, consistent with an assumed fracturing envelope parallel to the failure envelope. However, this concept and its physical significance in rock mechanics is not clearly understood. Although the permeability increase associated with dilatancy is a common phenomenon observed in laboratories (see [28]), some new tests of permeability measurements under controlled stress regime and fluid pressure are critically necessary.

Contrary to the modeling of Roberts and Nunn [2], our fracturing modeling results in a nearly continuous evolution due to its origin in fluid overpressuring. However, we cannot refute the possibility of episodic fracturing that would generate fractures opening during geologically long periods and would result in large quantities of fluid release and serious pressure drops. But we suggest that such episodic fracturing would be characterized by a larger size and would probably be associated with active tectonic environment.

Acknowledgements

The authors thank deeply B. Celerier for his important suggestions and English polishing. C. Sejourne, D. Fourmaintraux and W. Yang are thanked for their discussions and suggestions. Two reviewers, T. Engelder and Y. Gueguen, are specially thanked for their comments and constructive discussions and suggestions. This study is financially supported by the National Major Fundamental Research and Development project of China (No. G1999043310), by the National Natural Science Foundation of China (No. 49732005) and partly by Elf Aquitaine and Centre National de la Recherche Scientifique (PNRH Publ. No. 304).*[AC]*

References

[1] K. Magara, Compaction and Fluid Migration, Practical Petroleum Geology, Elsevier, Amsterdam, 1978, 319 pp.
[2] S.J. Roberts, J.A. Nunn, Episodic fluid expulsion from geopressured sediments, Mar. Pet. Geol. 12 (1995) 195–204.

[3] M.J. Osborne, R.E. Swarbrick, Mechanisms for generating overpressure in sedimentary basins: a reevaluation, Am. Assoc. Pet. Geol. Bull. 81 (1997) 1023–1041.
[4] C.Y. Wang, X.N. Xie, Hydrofracturing and episodic fluid flow in shale-rich basins – a numerical study, Am. Assoc. Pet. Geol. Bull. 82 (1998) 1857–1869.
[5] T. Engelder, A. Lacazette, Natural hydraulic fracturing, in: Barton, Stephansson Eds.), Rock Joints, Balkema, Rotterdam, 1990, pp. 35–43.
[6] W.H. Fertl, Abnormal Formation Pressure, Implication to Exploration, Drilling, and Production of Oil and Gas Reservoirs, Elsevier, Amsterdam, 1976, 382 pp.
[7] D.A. Mendelsohn, A review of hydraulic fracture modeling – part I: general concepts, 2D models, motivation for 3D modeling, J. Energy Resources Technol. 106 (1984) 369–376.
[8] M. Bouteca, J.P. Sarda, Etat de l'art en fracturation hydraulique, Rev. Inst. Fr. Pét. 42 (1987) 39–75.
[9] M.K. Hubbert, D.G.W. Willis, Mechanics of hydraulic fracturing, Trans. Am. Inst. Min. Eng. 210 (1957) 153–168.
[10] M.K. Hubbert, W.W. Rubey, Mechanics of fluid filled porous solids and its application to over thrust faulting, 1, role of fluid pressure in mechanics of over thrust faulting, Geol. Soc. Am. Bull. 70 (1959) 115–166.
[11] B. Tissot, R. Pelet, Nouvelles données sur les mécanismes de genèse et de migration du pétrole: simulation mathématique et application à la prospection. Proceedings 8th World Petroleum Congress, vol. 2, 1971, pp. 35–46.
[12] J.C. Jaeger, N.G. Cook, Fundamentals of Rock Mechanics, Chapman and Hall, London, 1979, 593 pp.
[13] D.D. Pollard, A. Aydin, Progres in understanding jointing over the past century, Geol. Soc. Am. 100 (1988) 1181–1204.
[14] P. Ungerer, F. Bessis, Y. Chenet, B. Durand, E. Nogaret, A., Chiarelli, J.L. Oudin, J.K. Perrin, Geological and geochemical models in oil exploration: principles and practical examples, In: Demaison (Ed.), Petroleum Geochemistry and Basin Evaluation, Am. Assoc. Pet. Geol. Mem. 35 (1984) 53–57.
[15] I. Lerche, Basin Analysis, Quantative methods, vol. 1, Academic Press, San Diego, CA, 1990, 562 pp.
[16] P. Ungerer, J. Burrus, B. Doligez, Y. Chenet, F. Bessis, Basin evaluation by integrated two-dimensional modeling of heat transfer, fluid flow, hydrocarbon generation, and migration, Am. Assoc. Pet. Geol. Bull. 74 (1990) 309–335.
[17] J.M. Hunt, Generation and migration of petroleum from abnormally pressured fluid compartments, Am. Assoc. Pet. Geol. Bull. 74 (1990) 1–12.
[18] F.D. Cipriani, L.M. Cathle, P.D. Manhart, Simulating salt diapirism, overpressuring, and seal rupture in sedimentary basins, EOS 74 (1993) 155.
[19] J.A. Nunn, Buoyancy-driven propagation of isolated fluid-filled fractures: implications for fluid transport in Gulf of Mexico geopressured sediemnts, J. Geophys. Res. 101 (1996) 2963–2970.
[20] X.R. Luo, Modélisation des surpressions dans les bassins sédimentaire et des phénomènes associés, Ph.D. Thesis, University of Montpellier II, 1994.
[21] R.E. Chapman, Mechanical versus thermal cause of abnormal high pore pressure in shales, Am. Assoc. Pet. Geol. Bull. 64 (1980) 2179–2183.
[22] X.R. Luo, G. Vasseur, Contributions of compaction and aquathermal pressuring to geopressure and the influence of environmental conditions, Am. Assoc. Pet. Geol. Bull. 76 (1992) 1550–1559.
[23] X.R. Luo, G. Vasseur, Geopressuring mechanism of organic matter cracking: numerical modelling, Am. Assoc. Pet. Geol. Bull. 80 (1996) 856–874.
[24] O.L. Anderson, P.C. Grew, Stress corrosion theory of crack propagation with applications to geophysics, Rev. Geophys. 15 (1977) 77–104.
[25] J.E. Olson, Joint pattern development: effects of subcritical crack growth and mechanical crack interaction, J. Geophys. Res. 98 (1993) 12251–12265.
[26] W.F. Brace, B.W. Paulding, C. Scholtz, Dilatancy in the fracture of crystalline rocks, J. Geophys. Res. 71 (1966) 3939–3953.
[27] J.C. Lorenz, L.W. Teufel, N.R. Warpinski, Regional fractures I: a mechanism for the formation of regional fractures at depth in flat-lying reservoirs, Am. Assoc. Pet. Geol. Bull. 76 (1991) 1714–1737.
[28] Y. Gueguen, V. Palciauskas, Introduction à la physique des roches, Hermann, Paris, 1992, 299 pp.
[29] G. Simpson, Y. Gueguen, F. Schneider, Permeability enhancement due to micro-crack dilatancy in the damage regime, J. Geophys. Res. 106 (2001) 3995–4016.
[30] R.N. Schock, H.C. Heard, D.R. Stephens, Stress-strain behaviour of a granodiorite and two graywackes on compression to 20 kilobars, J. Geophys. Res. 78 (1973) 5922–5941.
[31] J. Handin, R.V. Hager Jr., M. Friedman, J. Feather, Experimental deformation of sedimentary rocks under confining pressure: pore pressure tests, Am. Assoc. Pet. Geol. Bull. 47 (1963) 717–755.
[32] R.O. Bredthauer, Strength characteristics of rock samples under hydraulic pressure, Trans. Am. Soc. Mech. Eng. 79 (1957) 695–708.
[33] D.T. Secor Jr., Role of fluid pressure in jointing, Am. J. Sci 263 (1965) 633–646.
[34] D.T. Snow, Anisotropic permeability of fractured media, Water Resources Res. 5 (1969) 1273–1289.
[35] B. Sagar, A. Runchal, Permeability of fractured rocks effect of fracture size and data uncertainties, Water Resources Res. 18 (1982) 266–274.
[36] X.R. Luo, J.H. Yang, Z.F. Wang, The overpressuring mechanisms in aquifers and pressure prediction in basins, Geol. Rev. 46 (2000) 22–31.
[37] X.R. Luo, G. Vasseur, Sealing efficiency of shales, Terra Nova 9 (1997) 71–74.
[38] M.D. Zoback, R.A. Stephenson, S. Cloetingh, B.T. Larsen, B. VanHoorn, A. Robinson, F. Horvath, C. Puigdefabregas, Z. Ben-Avraham, Stresses in the lithoshere and

sedimentary basin deformation, Tectonophysics 226 (1993) 1–13.
[39] D.M. Audet, J.D.C. McConnell, Forward modelling of porosity and pore pressure evolution in sedimentary basins, Basin Res. 4 (1992) 147–162.
[40] C.M. Bethke, Inverse hydrologic analysis of the distribution and origin of Gulf Coast-type geopressured zones, J. Geophys. Res. 91 (1986) 6535–6545.
[41] D.J. Grauls, J.M. Baleix, Role of overpressures and in situ stresses in fault-controlled hydrocarbon migration: a case study, Mar. Pet. Geol. 11 (1994) 734–742.
[42] M.D. Zoback, J.D. Byerlee, The effect of micro-crack dilatancy on the permeability of Westerly granite, J. Geophys. Res. 80 (1975) 750–755.
[43] M.D. Zoback, J.D. Byerlee, The effect of cyclic differential stress on dilatancy in Westerly granite under uniaxial and triaxial conditions, J. Geophys. Res. 80 (1975) 1526–1530.